Proton-helium correlation in 94 MeV/nucleon ^{16}O-induced reactions on Al, Ni, and Au targets

A. Badalá, R. Barbera, A. Palmeri, and G. S. Pappalardo
Istituto Nazionale di Fisica Nucleare, Sezione di Catania Università di Catania, Corso Italia 57, I95129 Catania, Italy

F. Riggi
Istituto Nazionale di Fisica Nucleare, Sezione di Catania, and Dipartimento di Fisica, Università di Catania, Corso Italia 57, I95129 Catania, Italy

G. Bizard, D. Durand, and J. L. Laville
Laboratoire de Physique Corpusculaire LA34-ISMRA, Institut National de Physique Nucléaire et de Physique des Particules, Centre National de la Recherche Scientifique, Université de Caen, 14050 Caen CEDEX, France
(Received 11 June 1991)

Azimuthal distributions of helium ions have been measured in coincidence with high-energy protons in reactions induced by ^{16}O at 94 MeV/nucleon on ^{27}Al, ^{58}Ni, and ^{197}Au. Helium ions have been detected in a large area multidetector. Protons have been observed at 90°. Mean multiplicities of light charged particles (H and He) are found slightly dependent on the target mass. Strong azimuthal asymmetries whose intensity is larger for the Al target and vanishes with the increasing of the target mass are observed in the He distributions. Experimental data are discussed in the framework of the participant-spectator picture of a modified fireball model, taking into account intermediate energy corrections. In this framework the behavior of the azimuthal asymmetries, as a function of the target mass, indicates a strong final-state interaction between participant and spectator fragments. Such a result is found in agreement with interaction time predictions of a microscopical calculation based on the Boltzmann-Nordheim-Vlasov equation.

PACS number(s): 25.70.Pq

I. INTRODUCTION

Heavy-ion reactions around 100 MeV/nucleon have been extensively studied for many projectile-target systems [1]. This phenomenology shows generally the fragmentation of projectile and target with the formation of a participant zone composed by strong interacting nucleons from the colliding nuclei. The excited fragments of nuclear matter move with velocities originating from the effective nucleon-nucleon collisions and decay mostly by emission of light particles.

These final products reflect the main characteristics of the three primary sources such as nuclear density, temperature, size, and lifetime [2]. The study of such products could give information on reaction mechanisms and source structure. One of the main interesting aspects of heavy-ion collisions is concerned with the study of the participant zone. Because of its violent birth, due to multiple collisions between nucleons from target and projectile, many degrees of freedom are involved and much energy is available in its own frame. It could evolve from high density and temperature to a cold state by emission of light particles. Experimental study of these final products could help in the understanding of this evolution.

Unfortunately a clean separation of the final products of a given primary source is not so easy experimentally. In any case, the final-state interaction of such products with massive residues could complicate the study.

In this energetic domain of heavy-ion-induced reactions, theoretical models [3] of the fragmentation process generally deal with two nuclear spectator fragments that are slightly excited and a participant fragment which is generated by the overlap of a part of the projectile and target nucleons. The participant fragment is generally very hot and generates by evaporation the large part of light particles observed in a collision.

However, the participant-spectator models do not take into account the final-state interaction between participant and spectator fragments, supposing that the freezing of the participant occurs when spectators are far away enough to avoid mutual nuclear interaction. On the contrary, this mutual interaction is in some way taken into account in dynamical models [4] such as that described by the Boltzmann-Nordheim-Vlasov (BNV) equation. Unfortunately such models are based on one-body theories and cannot describe complex fragments such as alpha particles. Then correlations between complex light particles cannot be discussed in the framework of such dynamical models.

Correlations between two light charged particles, emitted in heavy ion reactions at intermediate energy, have been extensively measured in order to study space-time configuration of emitting sources. These measurements have been performed by using light projectiles (^{12}C and ^{16}O) on a large variety of targets, spanning the whole stable mass range, in the incident energy dynamics between 25 and 50 MeV nucleon [5–7]. Physical processes as the projectile breakup processes were observed by

studying the emission of α particles in coincidence with projectilelike fragments [5]. Correlations between light particles have been measured also at large relative momenta [6,7]. Data on light targets show that the correlation function presents a maximum in a plane containing the beam axis. In the hypothesis of an isotropic emission in the frame of thermal-equilibrated sources the experimental evidences may be understood in terms of the phase-space constraints imposed by energy and momentum conservation on systems with finite number of nucleons [6,7]. For reaction on heavy targets, the two-particle correlations indicate an ordered transverse motion in the entrance channel reaction plane which is superimposed on the random velocities of the source constituents [6].

Preequilibrium two-particle correlation functions at large relative momenta have been studied in reaction induced by a heavy projectile at 60 MeV/nucleon [8]. The persistence of mean-field effects on the emitted correlated particles is analyzed.

Our experiment is concerned with the study of correlations between protons detected at a large angle and helium ions detected in a large zenith and azimuthal domain. We observe that the detected protons are essentially emitted by the participant zone because of their high kinetic energy and backward direction in the center-of-mass frame [9]. Detected helium ions are produced by the participant zone at all angles, but the main contribution at forward angles originates from spectator fragments of projectilelike type.

In a recent paper [9] such correlation has been studied for the Al target in a reaction induced by ^{16}O at 94 MeV/nucleon. Zenith and azimuthal distributions of He ions have been measured in coincidence with 150 MeV protons detected at 90°. Large azimuthal asymmetries of helium ions have been observed with a maximum yield in the plane defined by the beam axis and the proton detector, on the opposite side with respect to the high-energy proton. These asymmetries were interpreted as due to a source recoil effect caused by the large linear momentum of the emitted high-energy proton. Both proton and helium ions are produced by the same equilibrated source [10]. Hence, helium particles emitted after the proton reflect the sum of the original source velocity and the recoil velocity due to the emitted high-energy proton.

Data were compared to the prediction of a fireball statistical decay with a satisfactory reproduction of the absolute yields of both protons and helium particles as well as zenith and azimuthal distributions. Moreover, the applied model predicts very low impact parameters for collisions producing the high-energy protons. So, for the selected events, the source size exhausts almost completely projectile and target nucleons and spectator fragments are reduced to few nucleons. As a consequence, no interaction occurs between the participant and spectators. In this situation calculated energy spectra and angular distributions of particles emitted by the participant zone could be straightly compared to experimental data in order to extract physical informations on the reaction mechanisms and source characteristics.

The irradiation of heavier targets with a light projectile of 100 MeV/nucleon generally produces large targetlike fragments which in principle could give rise to a strong final-state interaction with the participant fragments. In this case, if the emission of light particles occurs before the complete separation of the participant from the spectator, their spatial and momentum distributions could be strongly distorted by the nuclear field of the massive spectator. The presence of such an effect could give information also on the emission time of observed light particles.

By using the method reported in Ref. [5] one can study the above-mentioned asymmetry as a function of the target mass. This implies the detection of the light particles emitted in coincidence with reaction products able to give a high recoil momentum to the residual source.

In the present work we report on proton-helium correlations in reactions induced by ^{16}O at 94 MeV/nucleon on Al, Ni, and Au targets. High-energy protons have been observed at large angles in order to select events in which they originate from the participant zone. Helium ions have been detected by a large-area multidetector able to measure their velocity and emission angle.

The aim of the present work is to discuss the dependence of the azimuthal asymmetry on the target mass and look for possible final-state interactions between participant and spectator fragments. This final-state interaction should strongly affect the spatial distributions of the emitted particles if their emission time is short enough. An evaluation of the emission time of light charged particles will be done by a dynamical model based on the BNV equation.

Section II is devoted to the description of the experiment. An overview of experimental results is presented in Sec. III. Data are discussed in the framework of a simple model based on a modified fireball geometry [11–13] coupled with the standard Weisskopf theory [14] of evaporation. Expectation of a dynamical model is discussed in Sec. IV. Section V is devoted to concluding remarks.

II. EXPERIMENTAL SETUP

The overall apparatus is sketched in Fig. 1. Protons of energy ranging from 20 to 150 MeV were detected by a range telescope of ten NE110 plastic scintillators in a 58.8 msr solid angle, at laboratory angle of 90°. Identification of protons was performed by means of energy loss in a multiple ΔE-E analysis. The mean energies of protons stopped in each element, starting from the third one, were 27.4, 43.2, 66.5, 91.2, 113.3, 132.5, and 149.9 MeV. Protons of energy higher than 158.2 MeV, crossing the last element of the telescope, were identified only by their energy loss.

The telescope detector is not able to resolve the energy loss of a proton and a deuteron. However, for protons of energies greater than 150 MeV, we assumed that deuteron contamination (whose corresponding energy for the same range is 200 MeV) is negligible. Our assumption is supported by measurements reported in Ref. [15] from which we can deduce that deuteron cross section is less than proton one by more than one order of magnitude. For low-energy protons ($\sim$27 MeV) the deuteron con-

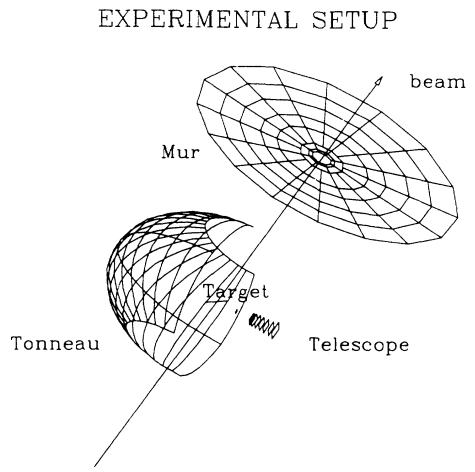

FIG. 1. Experimental setup. The telescope used as trigger for the "mur" and "tonneau" was located at the azimuthal angle $\phi=0°$. The "mur," consisting of seven rings of plastic scintillators (96), covered the angular range between 3° and 30°. Only half of the standard detector "tonneau" has been used in the present experiment. It consists of two groups of 18 staves covering the angular range 30°–90° and 90°–150°. Its azimuthal acceptance was of ±90° around $\phi=180°$.

tamination is about 20%. Results of calculations, obtained employing the model described in Sec. III, give indications similar to Ref. [15].

Light fragments were detected by two large-area multidetectors able to identify their charge Z, from hydrogen to oxygen, by a ΔE and time-of-flight (TOF) technique. The TOF start was given by the hf signal delivered by the machine. These multidetectors were the "mur" [16] (plastic wall) and a half part of the "tonneau" [17] (plastic barrel) installed in the vacuum chamber "Nautilus" at the GANIL facility.

The "mur" consists of an array of 96 plastic scintillators, 2 mm thick, arranged in seven concentric rings located at the angles 4°, 6°, 8.5°, 12°, 16.5°, 21.5°, and 27°, covering the whole azimuthal angle with a total solid angle of 0.85 sr. All the counters were placed 210 cm from the target position.

Large angles, from 30° to 150°, were covered by the "tonneau" which consists of 36 "staves" or plastic scintillators 2 mm thick. The "tonneau" was located on the opposite side of the telescope with respect to the beam as shown in Fig. 1; it covered an azimuthal angular range of 180° in steps of 10° with a total solid angle of 5.44 sr. Every plastic stave was located at a distance of 80 cm from the target. The light output of each scintillator was monitored at both ends by a photomultiplier. This allowed a determination of the crossing point of the charged particle through the transit duration time difference (t_1-t_2) of the light signals as measured at the two extremities. The uncertainty in the polar angle evaluation was about ±6°.

An aluminum foil, 200 μm thick, was placed in front of each plastic counter in order to absorb soft radiations. A very clean separation of the different charges was obtained only for particles crossing the scintillators, while the particles stopped in the detectors cannot be easily identified. An energy threshold of about 15 MeV/nucleon for H and He ions was thus imposed due

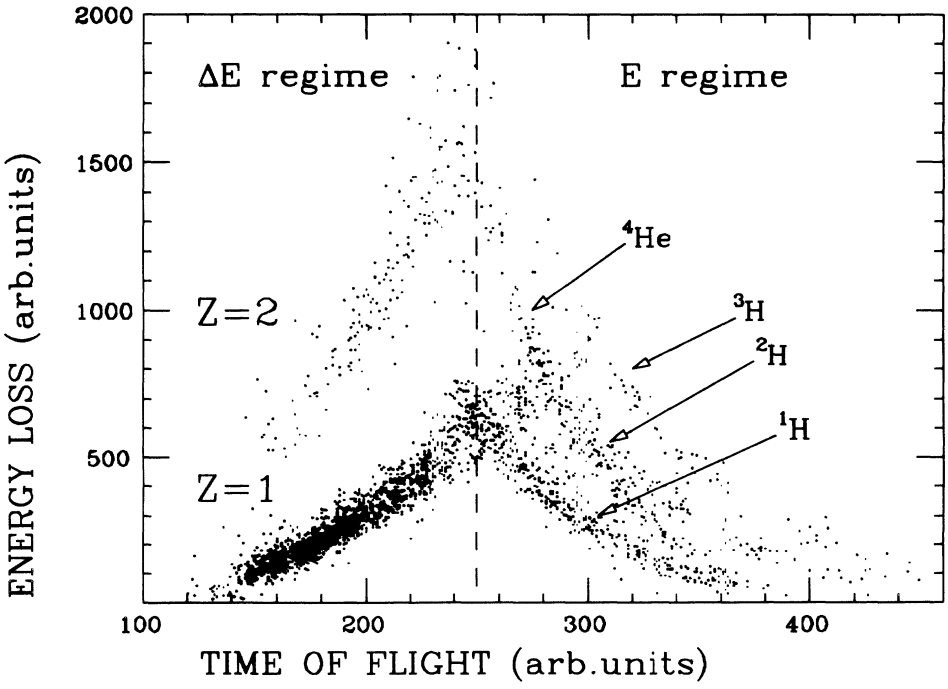

FIG. 2. Typical energy loss vs time-of-flight plot (ΔE-TOF) of a "tonneau" stave. On the left-hand side of the dashed line (which corresponds to a stopping range of 15 MeV/nucleon for protons and helium ions), the particles cross the detector (ΔE regime). On the right-hand side the particles are stopped within the detector (E regime).

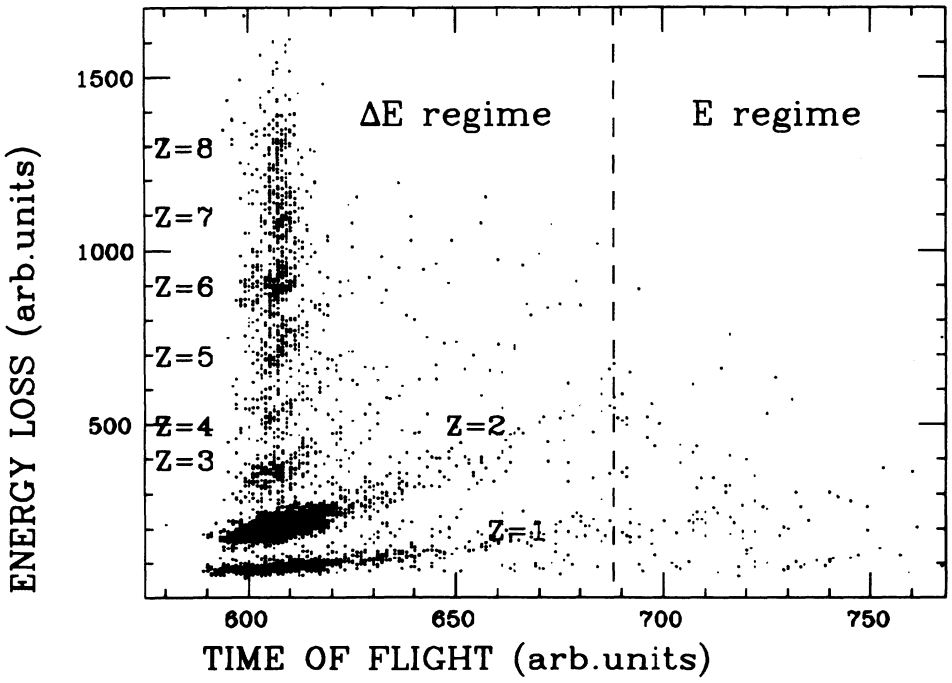

FIG. 3. ΔE-TOF plot from the "mur." As in Fig. 2 but for a plastic scintillator of the first ring (4°).

to the thickness of the detectors and of the aluminum foil absorber.

This 15 MeV/nucleon energy threshold was imposed in the data reduction for all physical quantities presented here, except for the multiplicity spectra shown in Figs. 10 and 11 (see next section), for which charge identification was not made. In Fig. 2 a typical ΔE-TOF plot for a "tonneau" stave is shown. $Z=1$ particles are clearly separated from $Z=2$ ones only in the ΔE regime. Figure 3 shows a ΔE-TOF plot for a counter of the first ring of the "mur," where charges from $Z=1$ up to $Z=8$ are visible.

The ^{16}O beam of 94 MeV/nucleon was pulsed with a repetition rate of 13.5 MHz. The FWHM of the beam pulse was 1 ns. Thicknesses of the targets were 6.76, 8.9, and 19.3 mg/cm^2 for ^{27}Al, ^{58}Ni, and ^{197}Au, respectively. The beam intensity was varied around 10^9 particles/s in order to limit random coincidences to about 10% of the number of true events. The present data are also corrected through the subtraction of random events.

III. EXPERIMENTAL RESULTS AND DISCUSSION

A. Velocity spectra

When a 150 MeV proton hits the telescope the helium ions are detected at all angles as allowed by the multidetector sketched in Fig. 1. In Figs. 4, 5, and 6 the measured helium ion velocity spectra at various polar angles are shown for the reactions ^{27}Al(^{16}O,pHe)X, ^{58}Ni(^{16}O,pHe)X, and ^{197}Au(^{16}O,pHe)X, respectively. Results concerning the ^{27}Al target have already been published [9], but they are reported here for sake of completeness and compared with the predictions of a theoretical model different from that of Ref. [5]. Velocity distributions present a low velocity threshold (5 cm/ns) due to the cutoff in the TOF-amplitude scatter plot as described in Sec. II for a clear separation of charges $Z=2$ and $Z=3$.

Two components are evident in these velocity spectra [10]. The first one is centered around the expected projectilelike velocity and essentially appears at forward angles; the second component is attributed to the midrapidity source [9]. It is visible at all angles and becomes the main contribution when increasing the polar angle. Some particles from targetlike fragments could be present in these spectra. However, the relatively low excitation energy of the primary fragments coupled to the experimental high value of the velocity threshold strongly reduces such a contribution.

The first component vanishes with increasing the angle and could be assumed completely absent at angles greater than 20°. This assumption seems quite reasonable if one considers that the grazing angles for the reactions induced by the ^{16}O at 100 MeV/nucleon on all targets are lower than 3°. In the following the experimental data will be compared to fireball model calculations which do not contain detailed information on the projectilelike fragments. In order to compare the data to these calculations, for some observable, only light particles emitted at very large angles will be considered. By taking into account only light particles emitted at angles greater than 20° one can deduce physical information on the midrapidity source.

Histograms in Figs. 4, 5, and 6 represent the produced velocity spectra as calculated by the modified fireball model (MFM). This model has been extensively used [10,18,19] and in the present work we mention only their

main characteristics and ingredients employed in the estimation of the calculated fireball. The MFM is based on the geometric fireball [20] model (GFM) which calculates, by a geometrical approach, the nuclear matter overlap between projectile and target at each impact parameter. Such a geometry defines the total number of nucleons which generate a hot source at an excitation energy roughly defined by the kinetic energy transferred from the projectile nucleons to the participant zone.

The MFM modifies the size and energetics of the geometrical fireball by taking into account the so-called *intermediate energy corrections* [11–13] such as Pauli blocking and one-body dissipation. These effects noticeably modify the nucleon number and the excitation energy of the hot source: (i) the number of participant nucleons is reduced in comparison with the geometrical abrasion value; (ii) the fireball energetics are also affected since some energy is dissipated in the spectators through a nucleon exchange mechanism. The resulting participant zone has less nucleons than the geometrical fireball, but with a higher excitation energy per nucleon. For a detailed presentation of the MFM see Refs. [12–14].

For the three targets, the calculated fireball size and excitation energy versus the impact parameter is shown in Figs. 7 and 8, respectively. The relative large difference of fireball sizes calculated by the GFM and the MFM is evident.

In order to compare calculations with experimental data we use a standard sequential decay of fireballs, namely, the Weisskopf theory of freezing a hot and equilibrated source. This approach has been successfully employed elsewhere in various studies of energetic radiation production as pions [10,18,19], high-energy protons [4,19], and gamma rays [12]. The sequential decay of the equilibrated source at each impact parameter includes only neutrons, protons, deuterons, tritons, ^{3}He, and ^{4}He. This is justified by the strong decrease observed for the multiplicities of particles with a Z larger than 2 which are not discussed in the present work.

As it is difficult to calculate analytically these many-body observables, we are led to perform a complete simulation of the decay process by means of a Monte Carlo method. To do this, we calculate at each step of the process the partial width for the emission of each type of particle. According to these widths, a particle is chosen and its velocity is randomly selected from a thermalized distribution according to the temperature of the system at the step under consideration. The emission of the trigger (a proton of 150 MeV) is considered at each step by a perturbative way, thus correctly counting the first, second,...,nth chance of emission up to 20th. Momentum and energy conservation are correctly treated at each

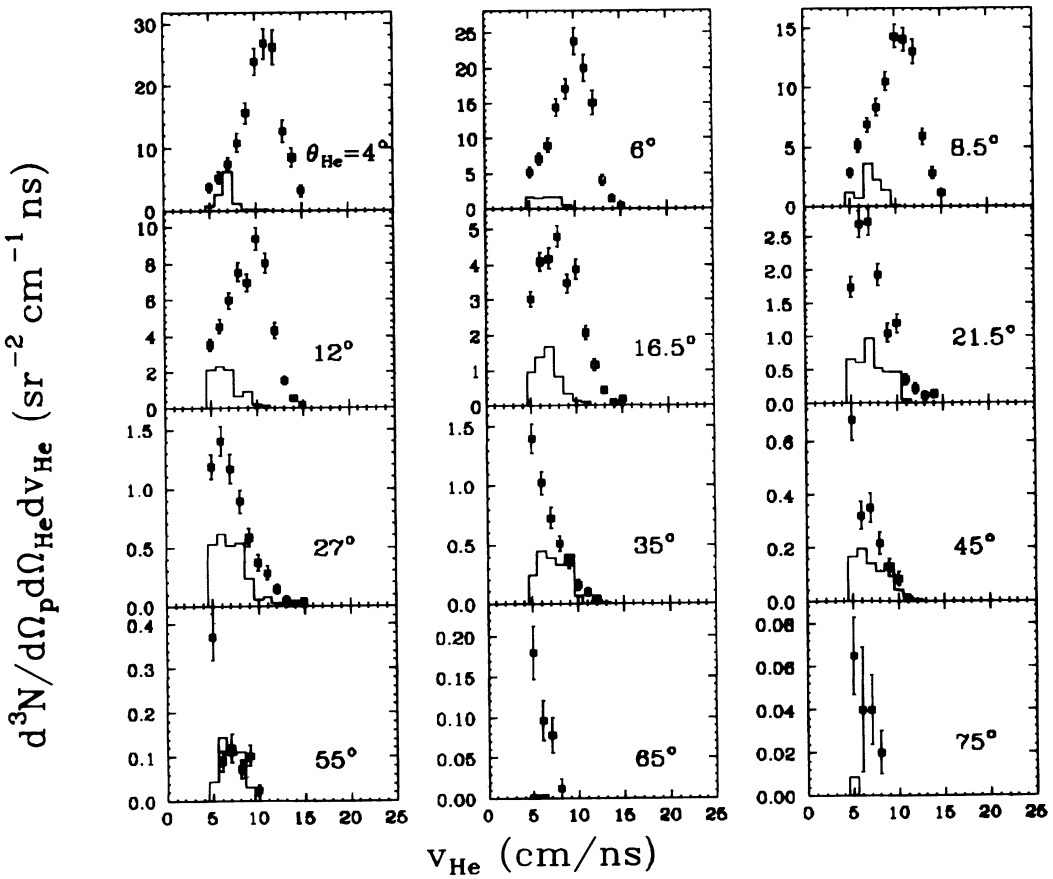

FIG. 4. Velocity spectra of $Z=2$ particles in coincidence with 150 MeV protons detected at 90° relative to the ^{27}Al target. The histograms are the velocity spectra calculated with the MFM (see text).

step of the decay. In order to allow for a direct comparison with the experimental data, the detector geometry as well as the velocity threshold are considered in the simulation. Comparison of present calculations with experimental velocity distributions, shown in Figs. 4, 5 and 6, evidences an overall agreement. Yields and shapes of velocity distributions are satisfactorily reproduced apart from the experimental contribution due to the projectilelike component.

The obtained high-energy proton yield distributions, versus the impact parameter, for the different systems, are shown in Fig. 9. Continuous and dashed lines refer to the MFM and GFM, respectively. Then the relative yields of protons at 90° for the three targets and for the two models are simply obtained by integrating the histograms.

B. Multiplicity distributions

We now report on the multiplicity of all detected charged particles in events producing the triggering proton. The experimental multiplicity distributions measured by the used multidetector of Fig. 1 are shown in Fig. 10 for the three targets. Multiplicities are obtained without any identification of the various charged particles present in selected events. Then the threshold of 5 cm/ns used for the charge identification is not introduced.

These distributions contain all detected particles which originate from all possible sources, namely, participant zone as well as targetlike and projectilelike fragments. The similarity of these distributions does not, however, indicate that the sources of light charged particles in these systems are strictly similar. In fact, velocity distributions of Figs. 4, 5 and 6 show differences in the helium yields at the same angle for the various targets. The main difference is due to the projectilelike helium particle contribution which diminishes at forward angles when increasing the target mass.

In order to clean these multiplicity distributions from contributions originating from the projectilelike fragment we take into account only particles detected in the "backward" direction ($\theta \geq 20°$). This angle is not a critical one but in the velocity distributions, the complete disappearance of the high-velocity components attributed [9] to the projectilelike emissions, can be observed at angles larger than 20°. The resulting multiplicity distributions are shown in Fig. 11. Very little differences in shape and mean value are observed in the three distributions. That relative to the Al target shows a maximum located at the multiplicity value one unit less than the other targets. No substantial differences are observed in the two multi-

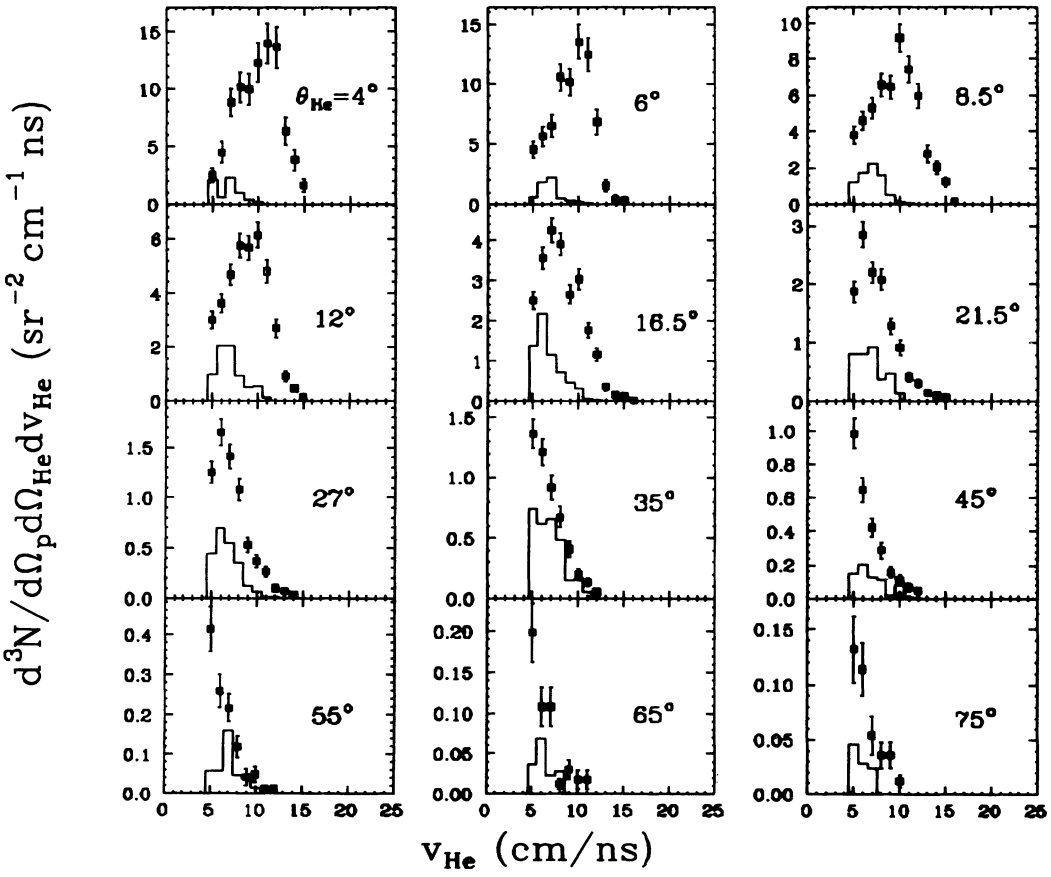

FIG. 5. As in Fig. 4 for the ^{58}Ni target.

plicity distributions relative to Ni and Au targets. Obviously because of the specific geometry and granularity of the employed multidetector and because of the limited angular domain taken into account in the evaluation of multiplicity distributions it is hard to deduce information on the absolute size of the emitting sources. However, in principle, relative mean multiplicity values or differences in shapes could be related to differences in the source characteristics, namely sizes and excitation energies. From the experimental multiplicity distributions relative to the three targets one can only conclude that source sizes and energetics are not much different.

For a better estimation of the relative source characteristics one can compare the experimental response of the used multidetector with that calculated by simulation of the decay of given sources with assumed sizes and excitation energies. To do this, we estimated the mean number of nucleons of the fireballs producing a triggering proton by using calculations reproduced in Fig. 7 and Fig. 9.

By folding the $A_{\text{fire}}(b)$ (Fig. 7) function with the yield distributions $d\sigma/db$ of Fig. 9, we obtain the $\langle A_{\text{fire}} \rangle$ values reported in Table I. The broad range of values for the mean nucleon numbers of fireballs, for the three targets, calculated with the GFM is evident. On the contrary, predictions of MFM show that size differences lie

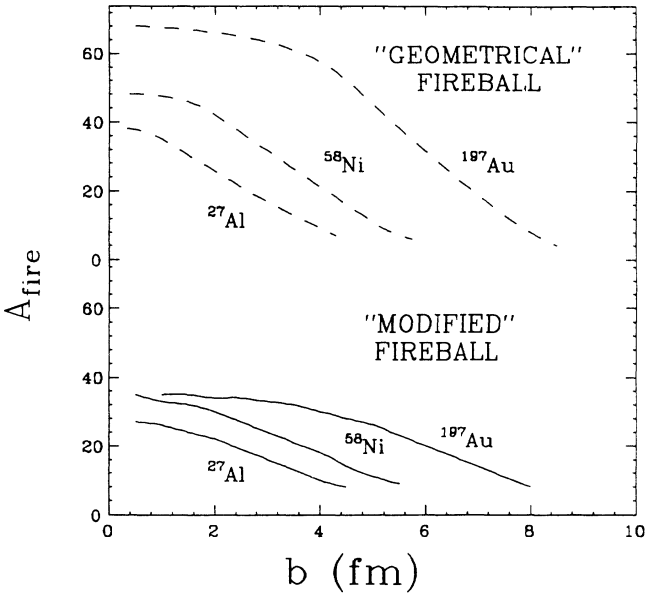

FIG. 7. Mass number A_{fire} of the fireball vs the impact parameter for the reactions induced by ^{16}O on the used targets. Dashed and full curves are relative to GFM and MFM, respectively (see text).

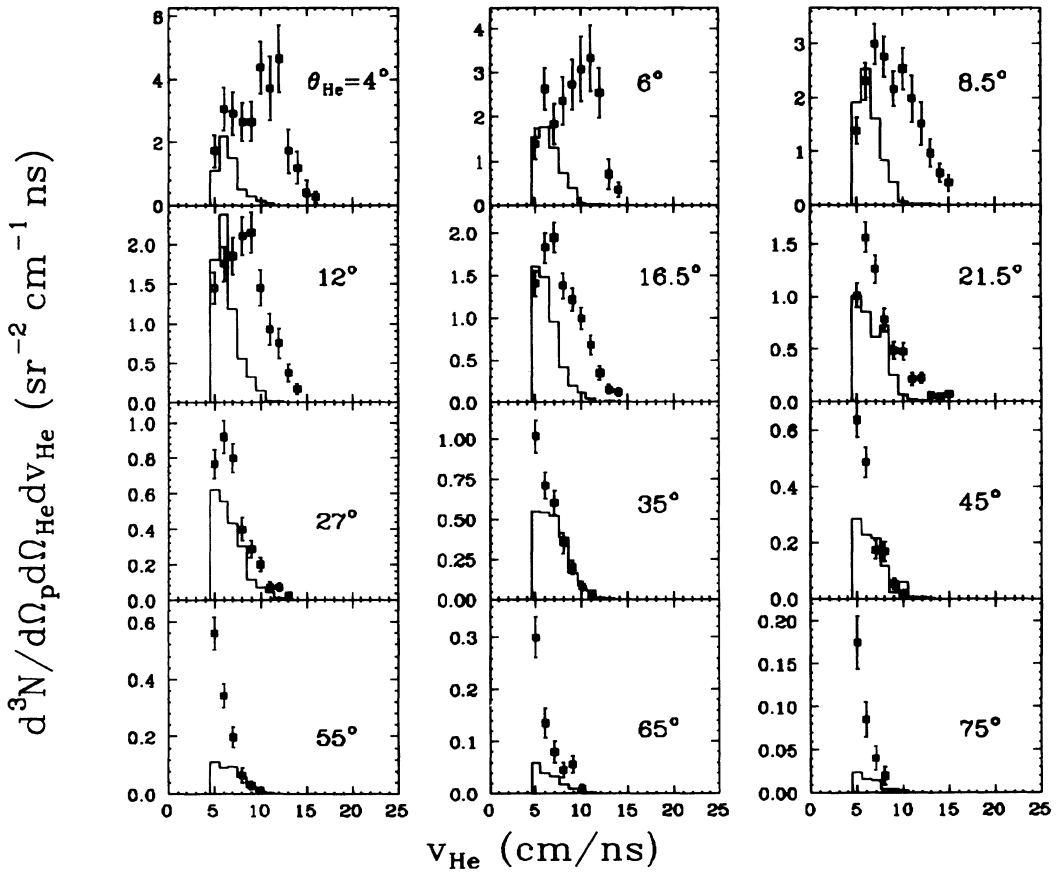

FIG. 6. As in Fig. 4 for the ^{197}Au target.

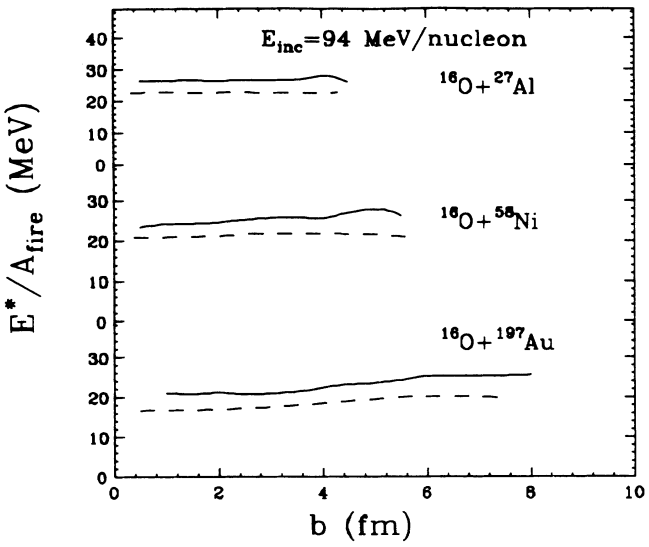

FIG. 8. Excitation energy per nucleon of the fireball, vs the impact parameter, for the reactions induced by a 94 MeV/nucleon ^{16}O on the used targets. Dashed and full curves are relative to GFM and MFM, respectively (see text).

within 20% of the total nucleon number.

Because of the flat distributions of the excitation energy as a function of the impact parameter the $\langle E^*/A_{\text{fire}} \rangle$ mean value weighted by the yield distributions of Fig. 9 is immediately deducible from Fig. 8. It is easy to conclude that mean multiplicities calculated with the *modified fireball* model increase very slowly with the target mass. Moreover, because of the decrease of the excitation energy of the fireball with the target mass one should expect a low dependence of the total number of emitted particles for the irradiated targets. Multiplicity predictions of GFM should show consistent differences with the target mass.

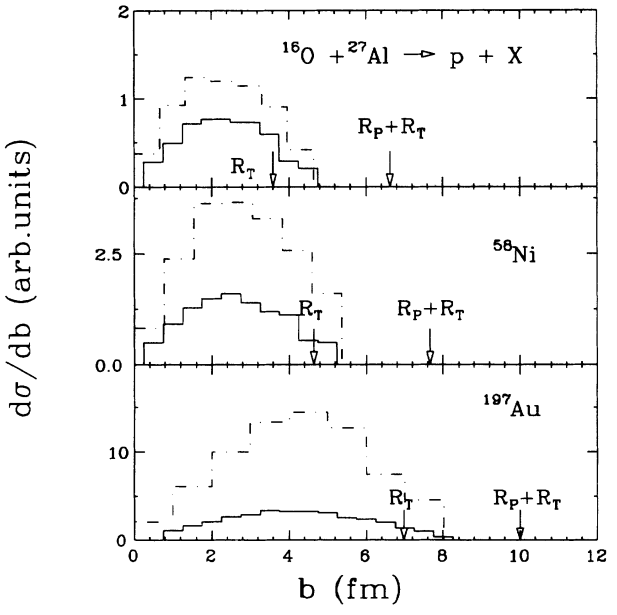

FIG. 9. Impact parameter dependence of the emission rate of a 150 MeV proton at 90° from the reactions induced by a 94 MeV/nucleon ^{16}O on the ^{27}Al, ^{58}Ni, and ^{197}Au targets. R_P and R_T are the projectile and target radii, respectively.

TABLE I. Mean value of fireball nucleon number, for the three targets, as predicted by the GFM and MFM (see text).

Target	$\langle A^{\text{GFM}} \rangle$	$\langle A^{\text{MFM}} \rangle$
^{27}Al	23.1	20.5
^{58}Ni	32.9	25.4
^{197}Au	49.4	27.4

The experimental multiplicity distributions for particles emitted at angles greater than 20° for Al, Ni, and Au are shown in Fig. 11. The calculated charged particle multiplicity distributions with the two models are shown in Figs. 12 and 13, respectively. A remarkable agreement in shape and relative value of the *modified fireball* distributions with the experimental ones is found. Relatively to the predictions of the *geometrical fireball* it is hard to find some closing aspect with the experimental multiplicity distributions. However, we observe that data of Ref. [5], for the Al target, have been well reproduced by predictions of the sequential decay of the *geometric fireball.* This is not surprising because, as can be deduced by calculations reported in Figs. 7, 8, 9, and Table I, the fireball size and energetics, for this target, do not differ more than those calculated with the MFM model.

To conclude this section we state that, for the reaction induced by ^{16}O at 100 MeV/nucleon and for the irradiated targets, the so-called fireballs are almost equal in size and excitation energy. This conclusion is the consequence of the agreement of the experimental multiplicity distributions with the MFM multiplicity predictions.

C. Azimuthal distributions

Conclusions of the previous section will be used here to discuss the behavior of asymmetries observed in the spatial distributions of helium ions when they are produced in collisions in which an energetic proton is detected at large angles. We assume that both high-energy protons and helium ions at angles greater than 20° are emitted by the same source, i.e., the fireball. Since the fireballs for the three targets have comparable sizes and excitation energies, one expects that recoil effects of the residual nuclear matter, after the emission of the proton, will be similar, at least in the absence of any final state interaction between these sources and spectator fragments.

Helium ion yields at various polar angles are reported in Fig. 14 as a function of the azimuthal angle ϕ. The intensity of the asymmetry depends on the polar angle and on the target. At low angles no large difference is observed between yields at $\phi=0°$ and $\phi=180°$ and, in principle, at $\theta=0°$ this difference should be zero within the statistical limits. With the increase of the polar angle differences become evident for all targets. However, while for the Al case this difference increases strongly with the polar angle, for the Au one such increase is not evident.

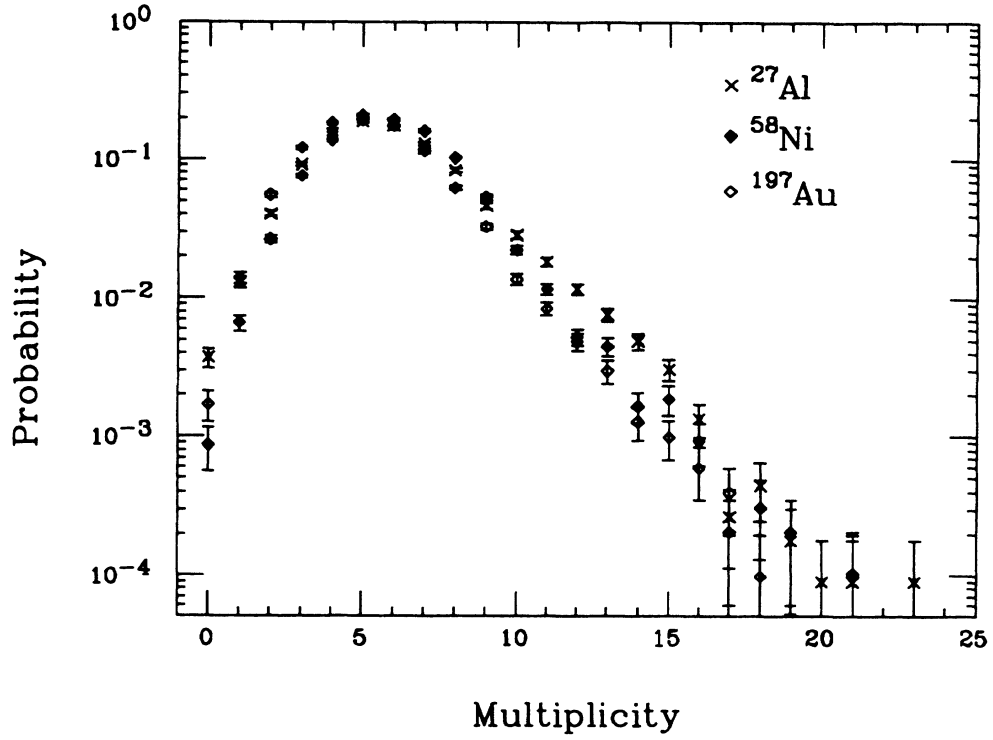

FIG. 10. Charged particle multiplicity distributions for the three irradiated targets, for events in which a 150 MeV proton has been detected at 90° and with the complete detection apparatus of Fig. 1.

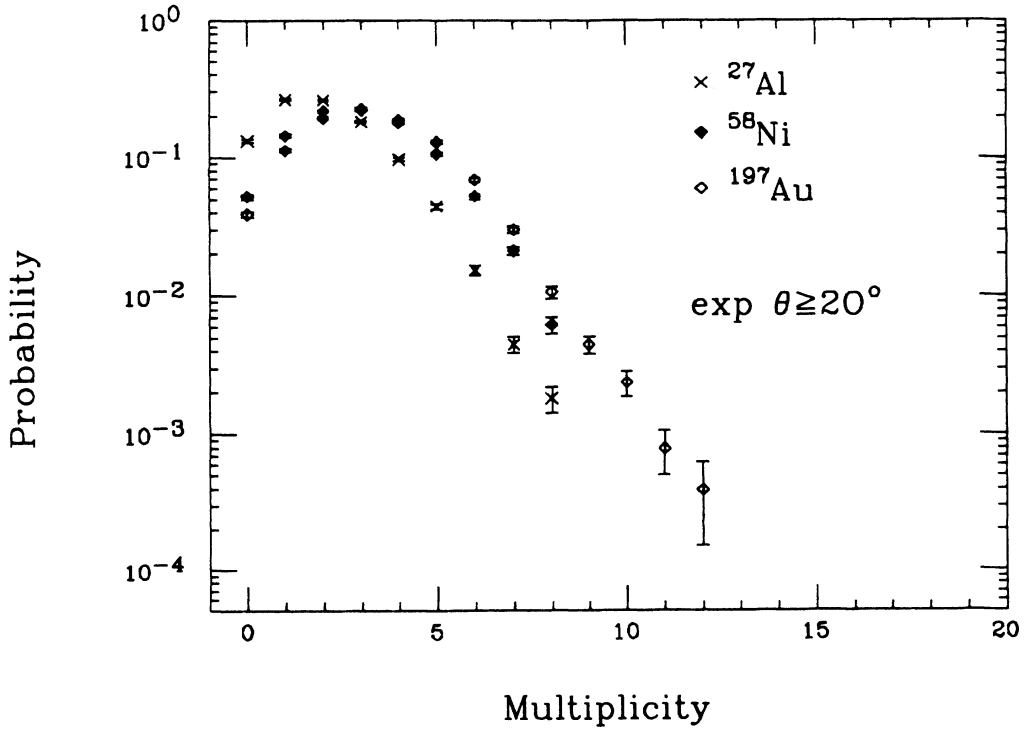

FIG. 11. Multiplicity distributions of charged particles hitting detectors at angles greater than 20°.

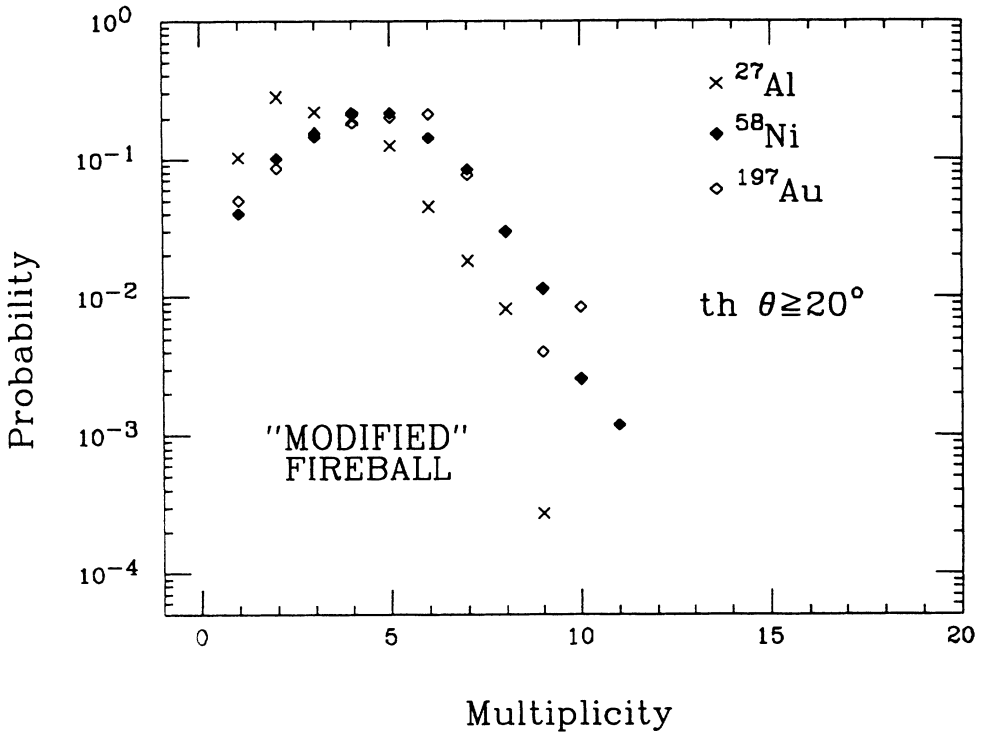

FIG. 12. Charged particle multiplicity distributions calculated by the simulation method described in Sec. III for the MFM. Only events in which a 150 MeV proton has been emitted at 90° have been taken into account and only particles produced at angles greater than 20° contribute to the shown distributions.

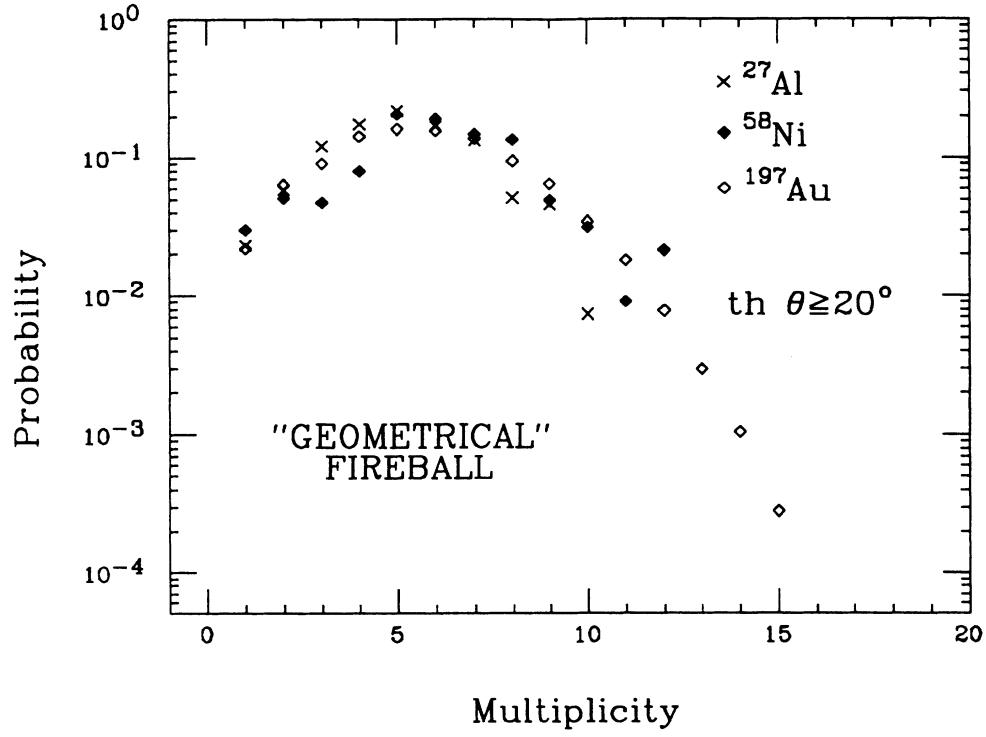

FIG. 13. As in Fig. 12 but calculations are relative to the GFM.

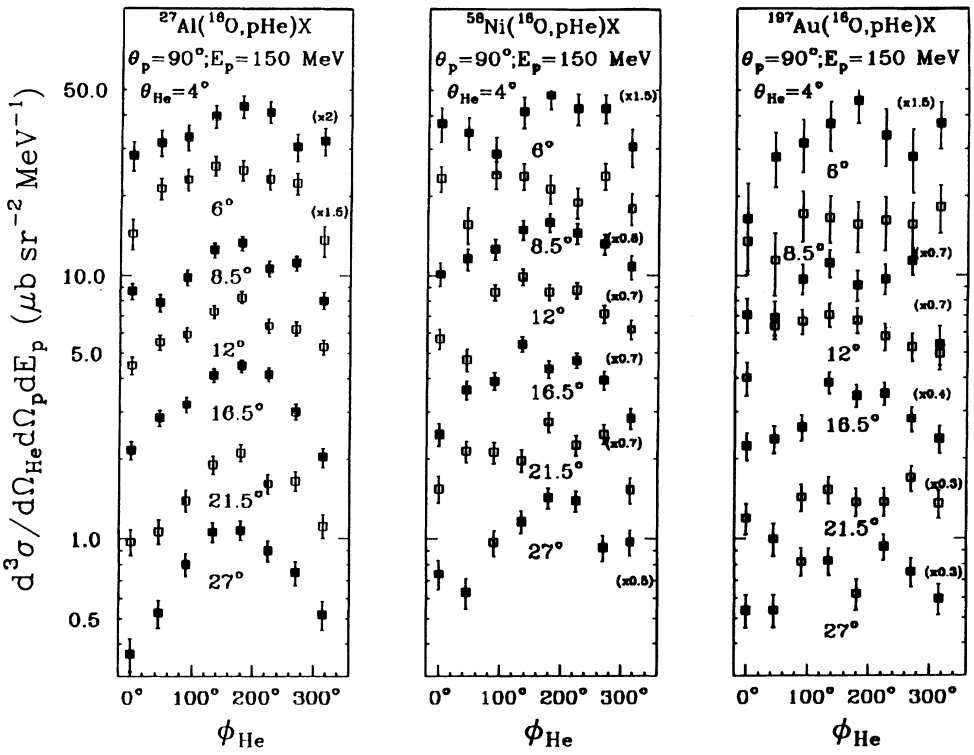

FIG. 14. Azimuthal distributions of $Z=2$ particles for 150 MeV triggering protons for the irradiated targets. Distributions are reported for various polar angles of the "mur."

The azimuthal distributions for the helium ions detected by the "tonneau" are also reported (see Fig. 15). This detector covers the azimuthal angular range between $\phi=90°$ and $\phi=270°$. However, because of the low statistics it is hard, in these cases, to say anything about the azimuthal distributions of the helium yields. In order to study quantitatively the behavior of the observed asymmetries, we extract from the experimental azimuthal distributions the ratio $R=[y(180°)-y(0°)]/[y(180°)+y(0°)]$ between yields at $\phi=0°$ and $\phi=180°$, at each polar angle θ, by a fitting procedure using the following analytical expression: $y=A+B\sin^2(\phi/2)$. The resulting R values, as a function of the polar angle, are shown in Fig. 16 for the three targets. Dashed lines in Fig. 16 indicate a linear fit of the obtained R values for the Al case and have been reported for the other targets for a relative comparison. The trend shows a decreasing intensity of the asymmetry with the target mass. The Au case, in particular, shows a flat distribution strongly different from the Al one. At 4° and for all targets, experimental distributions show an R value different from zero within the statistical errors. The decreasing of the asymmetry with the target mass should indicate an increase of the fireball size. In this case, in fact, the velocity of the recoiling source should diminish and kinematical effects generating the asymmetry should vanish. This explanation is, however, in contrast with the conclusions deduced from the charged particle multiplicity distributions relative to the three targets. These were compatible with source sizes not too much different for the three targets. A direct comparison of experimental R values with that calculated with the theoretical models used in previous sections is shown in the right side of Fig. 16. Full and open squares represent the calculated asymmetry by the MFM and GFM model respectively. As already observed for velocity distributions both calculations reproduce well data relative to the Al target. Large discrepancies of the MFM model predictions are indeed observed for heavier targets due to the relative smallness of the source sizes. The asymmetries predicted by the GFM, due to the greater source sizes, are closer to the experimental ones but the trend of R relative to the Au is incompatible with experimental data. In conclusion, it seems that the recoiling source must be larger than that predicted by the GFM and maybe all nucleons of projectile and target recoil as a whole. In the hypothesis that all pieces of nuclear matter, spectators and participants, are in reciprocal interaction during the emission of the high-energy protons, it is possible that any recoil effect is strongly reduced. In this picture the low value of the azimuthal asymmetry for the Au case could be explained.

This picture needs a very fast emission of the high-energy protons originating a recoil of the total system and an emission time of the same order of the interaction time between target and projectile. This scenario includes the possibility that also the projectilelike residues reflect a recoil effect. Indeed, at forward angles, where the projectilelike $Z=2$ fragments are observed with high intensity, the experimental R values are not compatible with the calculated one relative to the fireball only. This relatively high R value can be explained as due to the asymmetry generated by the projectilelike primary frag-

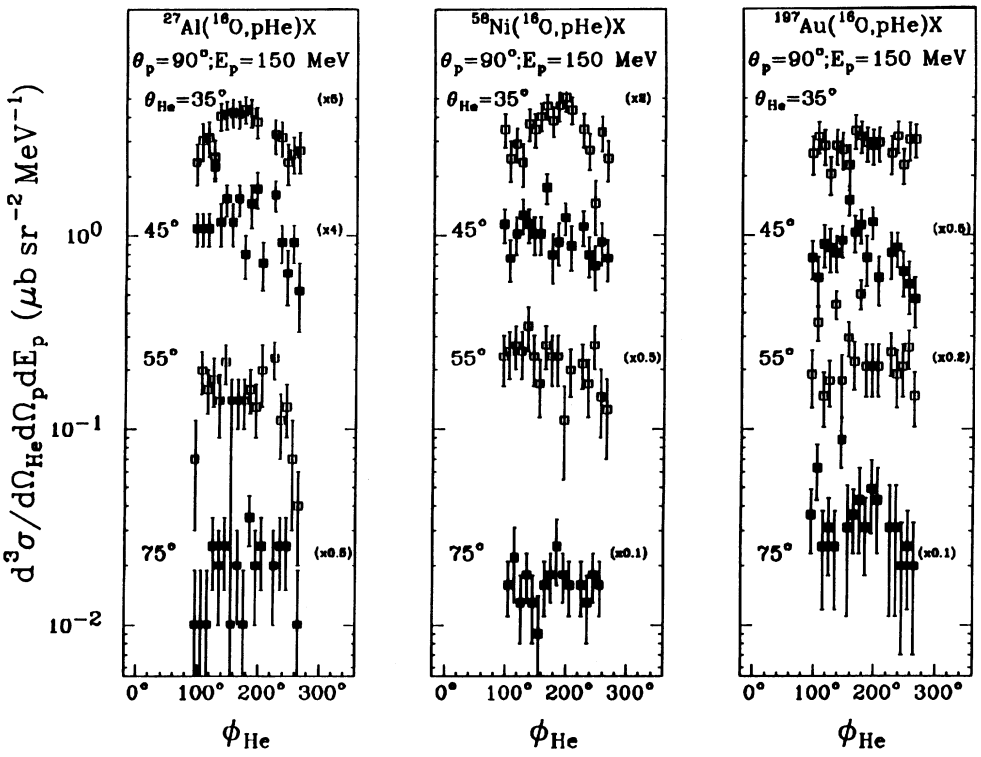

FIG. 15. Azimuthal distributions as in Fig. 14 but for polar angles covered by the "tonneau." The limited azimuthal range is due to the incomplete detector geometry (see Fig. 1).

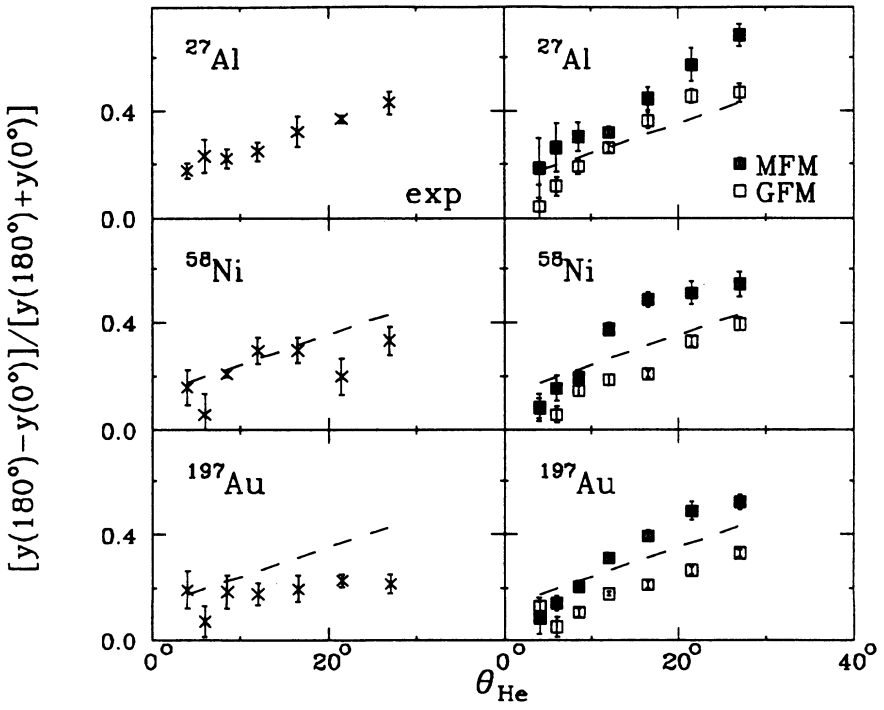

FIG. 16. Experimental asymmetry parameter (see text) vs the polar angle for all targets (left) and calculated asymmetry parameter (right). Full and open squares correspond to the MFM and GFM predictions, respectively. Dashed lines represent a linear best fit of the experimental ^{27}Al data and are reported on all figures as a guideline reference.

ments. In fact, because of the relatively low excitation energy of this primary fragments, the opening angle of the particle flow produced by its decay is not very large. In the hypothesis that this primary fragment undergoes a boost due to the detected high-energy proton, the produced asymmetry could be quite intense.

We conclude this section by extracting the two main aspects of the comparison between experimental and calculated data: light charged particles multiplicity distributions and spatial asymmetry of helium ions. The overall experimental features, velocity distributions of helium ions, multiplicity distributions, and absolute yield of 150 MeV protons [19] are reasonably reproduced by the MFM. Then sources producing high-energy protons and helium ions could decay in a sequential mode. Source sizes are slightly dependent on the irradiated target mass. Low azimuthal asymmetry shown in the Au case cannot be due to the recoil of the fireball as calculated by the MFM but probably to the strong interaction of this source with residual nuclear matter as the target spectator. In this picture the emission time of high-energy protons should be very short, of the same order of the interaction time of the target and projectile.

IV. DYNAMICAL CALCULATIONS

The time and space distributions of the emitting source can be exploited to a given extent by the use of dynamical models which in a natural way take into account the information on the position of the interacting nucleons in the phase space as well as the time evolution of the collision process. These models, which are based on the numerical solution of the Boltzmann-Nordheim-Vlasov equation, have been recently used to study the emission of hard photons [12] and pions [19].

For this reason a dynamical calculation was carried out by numerically solving the BNV equation with the test particle method [4]. The time evolution of $N(A_1+A_2)$ test particles (where A_1 and A_2 are the mass numbers of the colliding nuclei and N is the number of test particles per nucleon) was followed by assuming a Skyrme mean field with a $K=200$ MeV compressibility in the Hamiltonian equation of motion. Each test particle was represented by a Gaussian function to generate a smooth distribution in the phase space. Momentum changes of the test particles were considered to be due to individual nucleon-nucleon collisions. Nucleon emission was allowed for in the simulation by comparison of the kinetic energy of the involved particles and the Coulomb barrier and checking for the presence of other particles in the surroundings. About 100 test particles per nucleon were employed in the calculations reported here. Since the time evolution of the proton production does not depend too much on the impact parameter, calculations were performed at a given impact parameter, instead of integrating over b, as it is usual to evaluate absolute cross sections. However, to compare results on different targets, the impact parameters were chosen so as to give a nearly constant b/R_t value, R_t being the target radius.

Calculations were performed for low-energy ($E_p=30$ MeV) and high-energy ($E_p=150$ MeV) protons emitted at 90°, in order to look for possible differences in the corresponding emission times. Figure 17 shows the time evolution for the production of low-energy (left) and high-energy (right) protons for the three targets. As can be

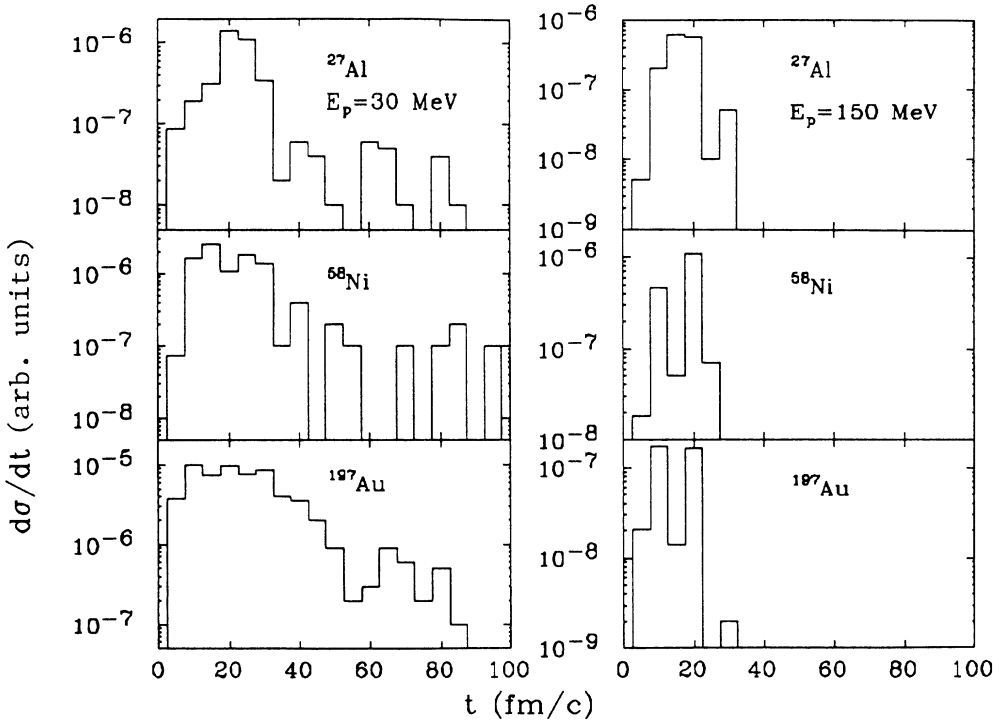

FIG. 17. Predicted time for the production at 90° of 30 MeV (left) and 150 MeV protons (right), for the reactions induced by 94 MeV/nucleon ^{16}O on various targets. Calculations have been made by a code based on the solution of the BNV equation (see text).

seen, all the contribution to the cross section for high-energy protons comes from the early stages of the interaction process (within ~20 fm/c), whereas low-energy protons can be produced also in a later stage, up to 40–50 fm/c. This is in agreement with what expected also for other energetic products, like pions [19]. Indeed, in a later stage of the interaction process, the phase space begins to be filled due to nucleon-nucleon collisions and the availability of final state phase space channels is greatly reduced. These times roughly correspond to traversed distances of about 8 fm for 100 MeV/nucleon ^{16}O ions, which are comparable with the size of the interacting system. This means that a strong overlap of the nuclear matter can be expected while the more energetic protons are being emitted, with a corresponding large final-state interaction between participant and spectator nuclei. This is confirmed by the spatial distribution of the interacting nucleons as derived by the BNV calculations.

The dynamical approach allows us also to follow the equilibration of the system. This parameter can be associated to the quantity $Q = 2\langle p_z^2 \rangle / (\langle p_x^2 \rangle + \langle p_y^2 \rangle)$, where p_x, p_y, and p_z are the ellipsoid axes in momentum space (z axis is taken along the beam direction). The evolution of this quantity with time is shown in Fig. 18 for the three targets. It can be observed from this result that a nearly

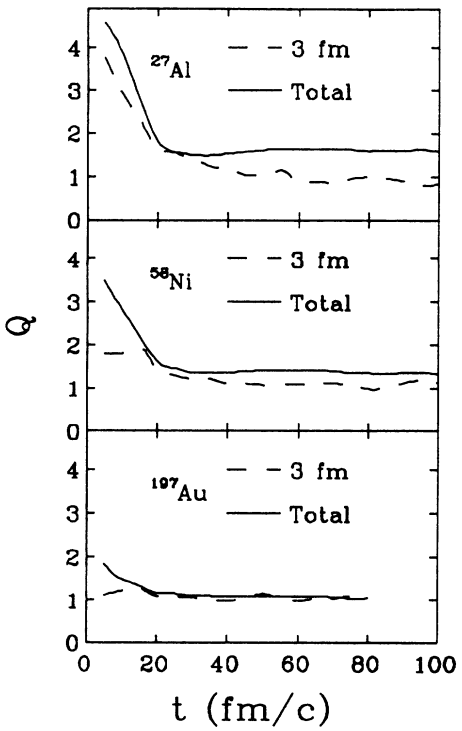

FIG. 18. Quadrupole deformation parameter calculated at 2, 2.6, and 3.9 fm for the Al, Ni, and Au targets, respectively. The chosen impact parameters for the three different targets keep constant the b/R_t ratio. The full line includes the total momenta of nucleons. Dashed line includes those nucleons contained in a sphere of 3 fm radius around the origin of the center of mass.

complete equilibration ($Q = 1$) is found for the Ni and Au case at times around 20 fm/c, when the emission of energetic protons is near its end. For the Al case, the quantity Q stabilizes at values greater than one. However, since the size of this fireball is smaller than the others, one should look to what happens in correspondingly smaller subsets of the spatial distribution. The same figure also shows the trend which was extracted from the dynamical calculations for the nuclear matter inside a sphere of 3 fm radius, showing that equilibration is achieved on the same time scale. The equilibration in such a relatively short time, predicted by the present dynamical calculations, justifies, in some way, the applicability of statistical models to a rather fast particle emission. Thus the rather good agreement of statistical calculations with experimental data is not surprising.

V. CONCLUSIONS

Three targets spanning a large range of mass have been irradiated with ^{16}O at 94 MeV/nucleon. Low-energy helium ions emitted from a source at intermediate rapidity have been observed in events in which a high-energy proton is emitted at large angles. Yields and velocity distributions of these particles are well reproduced by a fireball model which takes into account mean-field effects as well as the one-body dissipation and Pauli blocking. Spatial correlations between these two observed particles show that low-energy helium ions reflect a recoil effect due to the large linear momentum taken by a 150 MeV proton.

The multiplicity distributions of charged particles emitted by the fireballs relative to the three targets show that sizes and energetics of the emitting sources do not differ considerably with the target mass, thus suggesting that the number of participant nucleons of the equilibrated sources are almost the same, as it can be calculated by a modified fireball model (MFM).

On the contrary, the evolution of the azimuthal asymmetry in the spatial distributions of the helium ions, as a function of the target mass, is not compatible with this conclusion. In fact, the vanishing azimuthal asymmetry of the helium yields with the increasing target mass suggests that the recoiling nuclear matter should be very large for heavier targets compared to the source size extracted by experimental multiplicity distributions.

The apparent incoherence of these two aspects of the present data can disappear assuming that the emission of both high-energy protons and helium ions occurs during the interaction of the colliding nuclei when all projectile and target nucleons are in mutual interaction.

Indeed, emission time predictions, as well as phase-space distributions of nuclear matter, in dynamical model calculations show that high-energy proton emission is very fast compared to the interaction time of the colliding nuclei. In this time a large region of the nuclear matter is equilibrated allowing, in principle, for the emission of other particles such as helium ions. The description of bound complex fragments in these dynamical models is not yet done. Thus the correlation between

helium ions and other particles cannot be obtained within such a model, though calculations of many-body correlation in dynamical models now become available [21].

In conclusion, the data analysis of our experiment shows that kinematical effects such as the source recoil in particular heavy ion collisions could help in the understanding of the topology of the colliding zone. A correct and detailed description of the final-state interaction is then a strong constraint on the various theoretical models which would explicate the phenomenology of this kind of processes.

We are indebted to A. Bonasera and G. Russo for useful discussions and for the availability of some computer codes. We thank M. Di Toro for a critical reading of the manuscript. The Catania team thanks C. D'Amato, F. Librizzi, D. Nicotra, and C. Rapicavoli for their technical support.

[1] J. Sullivan *et al.*, Phys. Lett. B **249**, 8 (1990); K. Hagel *et al.*, Phys Lett. B **229**, 20 (1989); J. Peter *et al.*, Nucl. Phys. **A519**, 611 (1990); J. Mougey *et al.*, Phys. Lett. B **105**, 25 (1981).

[2] Z. Chen *et al.*, Phys. Rev. C **36**, 2297 (1987).

[3] S. Das Gupta and A. Z. Mekjian, Phys. Rep. **72**, 132 (1981), and references therein.

[4] G. Bertsch and S. Das Gupta, Phys. Rep. **160**, 190 (1988); W. Bauer, Nucl. Phys. **A471**, 604 (1987).

[5] P. L. Gonthier, P. Harper, B. Boums, R. Ramaker, D. A. Cebra, Z. M. Koenig, D. Fox, and G. D. Westfall, Phys. Rev. C **41**, 2635 (1990).

[6] M. B. Tsang *et al.*, Phys. Lett. **148B**, 265 (1984); C. B. Chitwood *et al.*, Phys. Rev. C **34**, 858 (1986).

[7] D. Fox, D. A. Cebra, J. Karn, C. Parks, G. D. Westfall, and W. K. Wilson, Phys. Rev. C **36**, 640 (1987); D. Fox, D. A. Cebra, J. Karn, C. Parks, A. Pradhan, A. Vander Molen, J. van der Plicht, G. D. Westfall, W. K. Wilson, and R. S. Tickle, Phys. Rev. C **38**, 146 (1988).

[8] D. Ardouin *et al.*, Nucl. Phys. **A514**, 564 (1990).

[9] D. Durand *et al.*, Nucl. Phys. **A511**, 442 (1990).

[10] R. Barbera *et al.*, Nucl. Phys. **A518**, 767 (1990).

[11] A. Adorno, A. Bonasera, M. Di Toro, C. Gregoire, and F. Gulminelli, Nucl. Phys. **A488**, 451c (1988).

[12] A. Bonasera, M. Di Toro, and C. Gregoire, Nucl. Phys. **A483**, 738 (1988); M. Prakash, P. Braun-Muzinger, J. Stachel, and N. Alamanos, Phys. Rev. C **37**, 1959 (1988).

[13] A. Bonasera, M. Di Toro, and C. Gregoire, Nucl. Phys. **A463**, 653 (1987).

[14] V. Weisskopf, Phys. Rev. **52**, 295 (1937).

[15] G. D. Westfall *et al.*, Phys. Lett. **116B**, 118 (1982).

[16] G. Bizard, A. Drouet, F. Lefebvres, J. P. Patry, B. Tamain, F. Guilbault, and C. Lebrun, Nucl. Instrum. Methods **A244**, 483 (1986).

[17] A. Peghaire *et al.*, Nucl. Instrum. Methods **A299**, 365 (1990).

[18] R. Barbera *et al.*, Nucl. Phys. **A519**, 231c (1990).

[19] A. Badala' *et al.*, Phys. Rev. C **43**, 190 (1991).

[20] J. Gosset, H. H. Gutbrod, W. G. Meyer, A. M. Poskanzer, A. Sandoval, R. Stock, and G. D. Westfall, Phys. Rev. C **16**, 629 (1977), and references therein.

[21] A. Bonasera and F. Gulminelli, Phys. Lett. B **259**, 399 (1991).